A 27-Mbps, 0.08-mm^3 CMOS Transceiver with Simultaneous Near-field Power Transmission and Data Telemetry for Implantable Systems

Jordan Thimot, Kukjoo Kim, Chen Shi, and Kenneth L. Shepard
Bioelectronic Systems Lab, Department of Electrical Engineering
Columbia University, New York NY

***Abstract*—This paper describes an inductively powered 27-Mbps, 0.08-mm^3 CMOS transceiver with integrated RF receiver coils for simultaneous two-way, near-field data telemetry and power transmission for implantable systems. A four-coil inductive link operates at a 27-MHz carrier for power and a 700-MHz carrier for data telemetry with the antennae taking an area of only 2 mm by 2 mm. Amplitude-shift-keying (ASK) modulation is used for data downlink at 6.6 kbps and load-shift keying (LSK) backscattering is used for data uplink at 27 Mbps. The transceiver consumes 2.7 mW and can power a load consuming up to an additional 1.5 mW. Implemented in a 0.18-um silicon-on-insulator (SOI) technology, post-processing steps are used to decrease chip thickness to approximately 15um, making the chip flexible with a tissue-like form factor and removing the effects of the substrate on coil performance. Power harvesting circuitry, including passive rectifier, voltage regulator, RF limiter, ASK and LSK modulator, clock generator, and digital controller are positioned adjacent to the coils and limited to an area of 0.5 mm by 2mm. Complete transceiver functionality of the system has been achieved with overall power transfer efficiency (PTE) of 1.04% through 1 mm of tissue phantom between reader and implant.**

Keywords—wireless power transmission; data telemetry; near-field inductive link; load-shift-keying; implantable medical devices; data equalization; power harvesting;

I. Introduction

Inductively coupled links have become commonplace in supplying both power and data to implantable medical devices (IMDs) [1,2,3,4]. Previous wireless IMDs have typically used off-chip receiver (Rx) antennas and circuitry for telemetry and voltage rectification, increasing the required volume of the implant considerably and creating a rigid interface between implant and tissue that triggers stronger immune response [1,2,3,4,5]. In our case, we seek to push down the scale and form-factor of RF transceivers and wireless powering to create millimeter-scale antennas for these links and do so on-chip, while achieving Mbps data rates and mW-scale power levels at mm-scale implantable depths. Other approaches for scaled power transfer such as ultrasound [6], which have advantages in implantation depth, do not allow high-data-rate telemetry because of MHz-scale carrier frequencies.

Our wireless implant has the Rx antennas integrated on-chip and, by thinning the substrates to 15µm, allows the implant transceiver to displace an overall volume of less than 0.08 mm^3 with the Rx coils covering an area of only 4 mm^2. Once thinned, the integrated transceiver has the form factor of tissue paper allowing it to conform to tissue surface. Removal of the lossy silicon substrates also improves wireless power transfer (WPT) efficiency.

The requirements for mW-scale power and Mbps-scale data rates necessitates the use of backscatter techniques (passive modulation of Rx resonance frequency) for data uplink (IMD to outside). Other high-data-rate telemetry techniques such as the use of ultra-wide-band (UWB) transmitters or non-passive frequency modulation, require larger antennas and power amplifiers to drive the antennas to achieve acceptable bit-error-rates (BERs) [5]. The use of millimeter-scale integrated coils produces smaller transmission radii and lower power transfer efficiency (PTE) than what would be achievable with larger, lower-loss antennae. Backscatter data transfer at high-data-rates with this antenna scale through lossy media, even at mm-scale implantation depths, also presents intersymbol-interference (ISI) challenges, which we overcome with extensive equalization of the channel.

II. Transceiver Design

A four-coil system is used for WPT and data telemetry with a fully integrated Rx fabricated in a 0.18µm silicon-on-insulator (SOI) technology (Fig. 1). Rx antennas are integrated with on-chip inductors of five and seven turns with outer diameters of 2mm and 1.2mm for power and data with inductor parameters specified in Table I. Total chip area is 5mm^2 including the on-chip inductors. Power is delivered at 27MHz and data is modulated onto a carrier frequency of 700MHz. Amplitude-shift-keying (ASK) demodulation circuitry (Fig. 2a) tracks the envelope of the data Rx's carrier signal for ASK downlink (external transceiver to IMD) transfer at 6.6kbps. Uplink data is sent through passive backscattering which modifies the resonance frequency of the data Rx using load-shift-keying

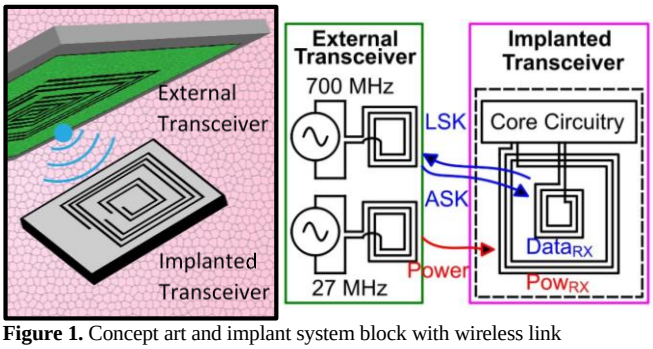

Figure 1. Concept art and implant system block with wireless link

978-1-7281-6031-3/20/$31.00 ©2020 IEEE

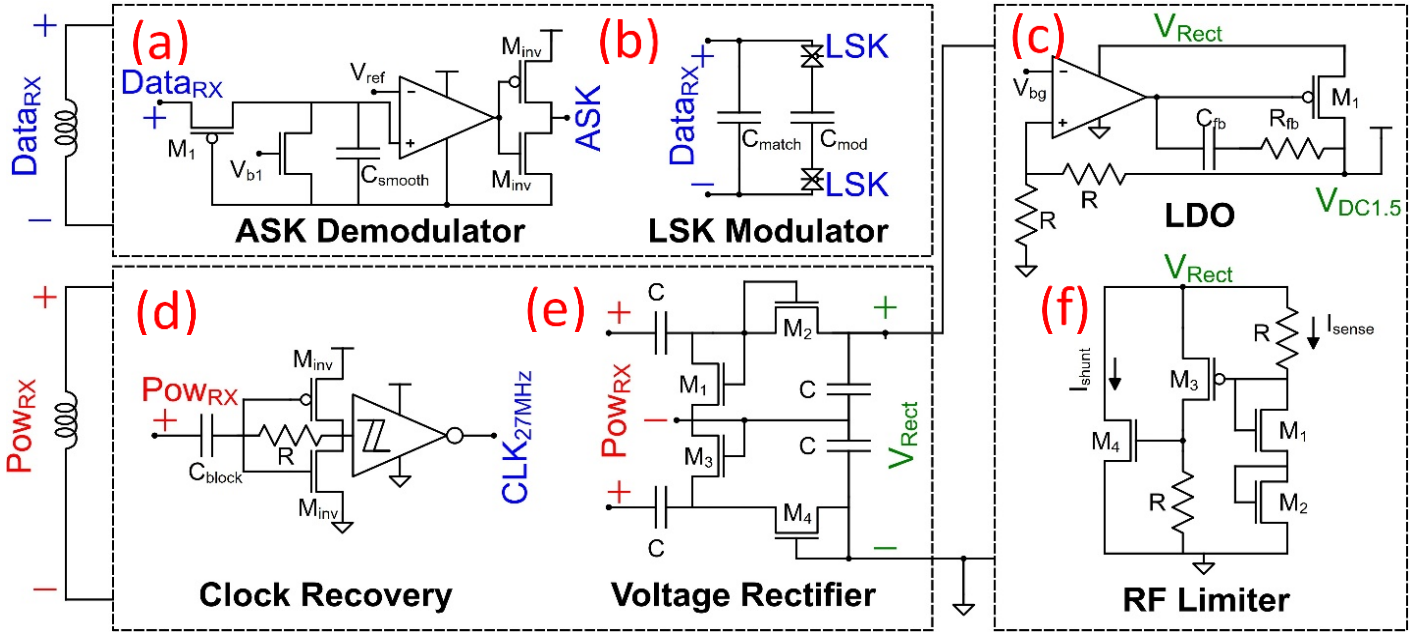

Figure 2. ASK demodulator (a), LSK modulator (b), LDO regulator (c), clock recovery (d), voltage rectifier (e), and RF limiter circuit topologies (f)

(LSK). LSK modulation circuitry (Fig. 2b) uses binary decisions to close pass gates which change the matching capacitance for the data Rx coil, effectively shunting the received 700MHz carrier signal to 0V. The external 700MHz transmitter (Tx) can detect this resonance shift in the form of a small increase in the amount of power output at 700MHz. The LSK modulation transmits data uplink at a rate of 27Mbps.

The power Rx is rectified with a passive voltage quadrupling topology (Fig. 2e), utilizing diode connected nFETs, which is used to power a low-dropout (LDO) linear regulator (Fig. 2c) with a minimum PSRR of 38dB from 10MHz-1GHz. Output voltage is regulated to 1.5V using a bandgap reference as a voltage reference, and the rectified voltage is kept within a range of 1.8V-1.95V by an RF limiter circuit (Fig. 2f) which shunts excess current if the input RF power levels exceeds 21.6mW. The total transceiver power is 2.7mW and can power a load of 1.5mW, for a total system power of 4.2mW. Simulated insertion loss for the power regulation system has a total RF-DC transfer efficiency of 40%, requiring 10.4mW of total WPT to implant. A clock recovery circuit (Fig. 2d) uses the power Rx signal to derive the 27-MHz clock by utilizing an inverter with resistive feedback and a buffered Schmitt trigger.

On start-up the implant enters a "blinking configuration" state. Since LSK transmission effectively shunts the received carrier signal to the no-amplitude condition to modulate a zero, only data uplink or downlink can occur at any given time. While in the blinking state, the implant alternates between transmitting the chip's current configuration settings for eight downlink cycles and listening for an ASK response. While listening, the LSK modulation circuitry is disabled. The external data Tx tracks this blinking state and sends the configuration word in the listening phase. If one of 16 valid words (which act as input configuration for the implant) is received, the implant enters the data transmit state where it continuously sends digitized data.

III. External Transceiver System

High-data-rate backscattering through lossy media presents ISI challenges for uplink data recovery using an integrated coil. The thickest metal layer is limited to 4µm in 0.18 µm SOI, giving the integrated coils low quality (Q) factors from small trace cross sectional area. Low Q decreases radiation efficiency, causing the received LSK signal to be >60dB lower than the transmitted 700MHz carrier. To overcome this, equalization techniques must be employed to process the LSK data and achieve acceptable BERs.

The external transceiver system (Fig. 3) is implemented with a 3.8-cm-by-3.8-cm transceiver board containing transmitter (Tx) antennas and power amplifiers capable of delivering 4 W of power to the antennas, a 8-cm-by-5-cm low-noise LSK recovery board which filters and down converts the LSK signal into the baseband, and a tethered motherboard which creates and transmits the data/power signals and digitizes the received LSK for equalization. Tx antennas are implemented as three-turn coils fabricated with the inductor parameters specified in Table I. The resulting data stream is sent to a Kintex-7 FPGA, which implements a modified-constant modulus algorithm (M-CMA) equalizer capable of real-time analysis of the LSK data stream. The measured BER of the complete link is better than $1x10^{-4}$, which there is room to improve with additional equalizer optimization. The BER of the link was determined using the known values from the blinking configuration state as a basis. Constellation diagrams and waveforms of the equalized signal at various stages of the M-CMA-algorithm are shown in Fig. 4.

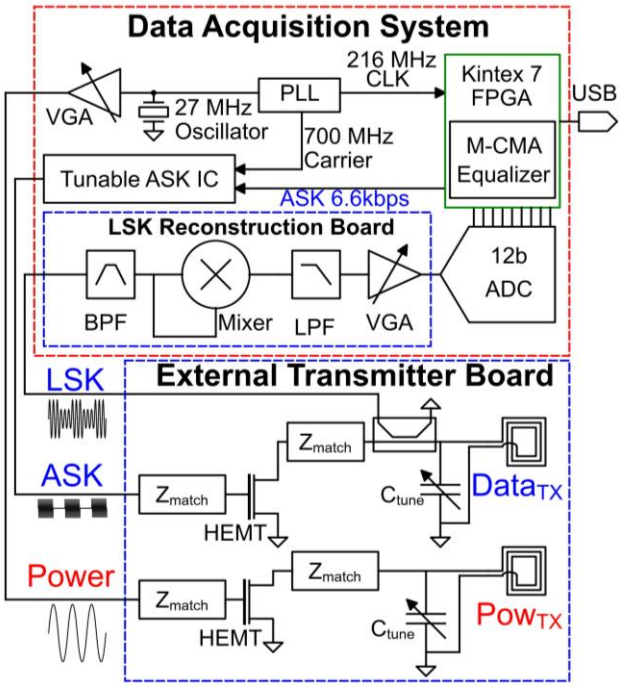

Figure 3. Data acquisition system block with external transceiver

The use of M-CMA here was driven by the unique requirements of this backscatter channel. Since the recovered LSK signal is incoherent and we do not have access to a training sequence, traditional adaptive filter techniques such as the least-means-square (LMS) or recursive-least-squares (RLS) algorithms are not possible. The constant-modulus algorithm (CMA) can recover incoherent signals without a training sequence, since its error function:

$$e(T) = |y_d(T)| - 1 \quad (1)$$

is only a function of the data decision $y_d(T)$. However, the use of self-mixing to demodulate the LSK signal only produces positive in-phase amplitude impulses for '0'-to-'1' transitions and negative in-phase amplitude impulses for '1'-to-'0' transitions that return to zero in-phase amplitude in two to three data cycles. The consequence is that three or more consecutive '0's or '1's become indistinguishable in amplitude, causing the CMA error function to fail. To correct this, the CMA error function is changed from adaptively forcing the data carrier to have a constant absolute value to only detecting if the current error function value is above or below the impulse threshold of a data transition. If the signal is above the threshold and of positive in-phase amplitude, the decision is a '1'; if of negative in-phase amplitude, the decision is a '0'. When the error function drifts below the threshold, we know the signal has settled back to zero amplitude but no change in data output has occurred. The M-CMA decision can be represented as:

$$y_d(T) = \begin{cases} 0,1 & e(T) > thres \\ y_d(T-1) & e(T) < thres \end{cases} \quad (2)$$

where the error threshold (*thres*) is tuned by an eight-bit user defined input constant, which varies based on Tx/Rx separation and the lossy medium. Because there are eight samples per symbol, a phase-picking algorithm takes the XOR of the current and previous M-CMA-decision to identify the time stamps of data transitions, recovering the phase of the incoherent signal and centering the FPGA clock to the data's phase. The M-CMA hardware was designed using MATLAB Simulink.

IV. Wireless Power Transmission and Data Telemetry

The four-coil near-field inductive link was designed using Mentor Graphics' IE3D method-of-moments solver. The power inductor pair was designed to operate at the 27-MHz ISM band, while the data inductor pair was designed to be matched at half the self-resonance frequency of the data coil (~700MHz), where a peak in inductor coupling is observed.

The implant is post-processed to remove most of the silicon substrate, greatly reducing chip volume (Fig. 5). The passivation, dielectric of the back-end stack, and silicon substrate are first trenched by dry etching, separating the transceiver from the rest of the die. Following this, the bulk silicon substrate is removed with plasma etching using the buried oxide layer as an etch stop, reducing overall thickness to 15 μm. At this thickness, the die has a flexible, tissue-paper-like form factor.

We can directly measure the S-parameters of the power coils for an unthinned die with 300 μm of 1000 Ω-cm silicon

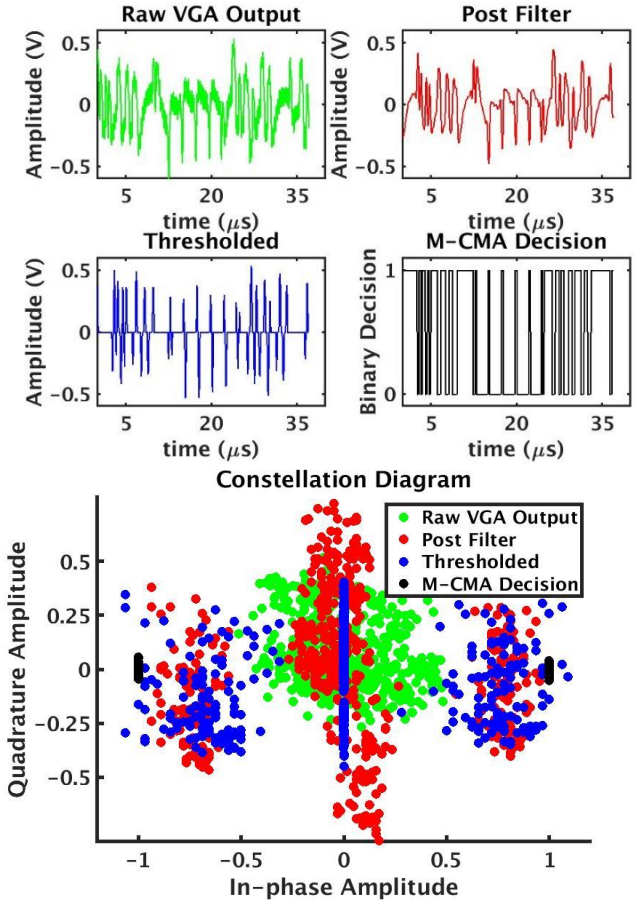

Figure 4: Waveforms and constellation diagrams of the raw oversampled VGA output (green), the post-filtered signal pre (blue) and post-application of error function thresholding, and the final M-CMA decision (black) during equalization.

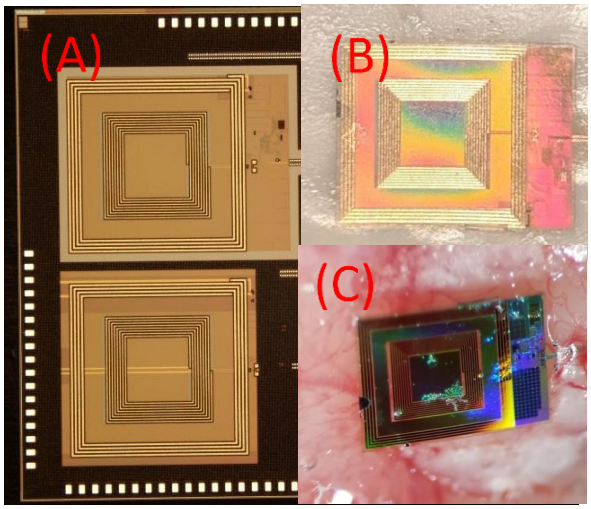

Figure 5. Photo of transceiver die as received from foundry (a), after post-processing and thinning (b), and after surgical implantation (c).

substrate present through direct wire bonds to the Rx coils. Measured S21 for WPT for an unthinned implant in air and phantom are comparable to ADS simulations at 1mm separation for a thinned implant transceiver (Fig. 6a). Direct WPT measurements for a thinned die is not possible as bond pads are cleaved from the chip; however, ADS simulations indicate an expected WPT increase of 1.1dB post thinning, which is consistent with observed coupling at the external transceiver. S43 simulations (Fig. 6c) for data coil coupling show a 30-dB decrease in received signal when the LSK is enabled, which is consistent with the observed amplitude shift in the backscatter LSK signal at the data Tx. The overall measured PTE of the link is 2.57% with 1mm of air separation and drops to 1.04% through a 1-mm gelatin phantom. Peak WPT from 1-5 mm of separation (Fig. 6b) show a decrease of 35dB from minimum to maximum separation. Beyond 2.5 mm the overall WPT drops below 0.1% where the external transceiver can no longer fully power the implant at this coil size.

V. Results and Conclusions

Transceiver operation has been verified through 1 mm of gelatin phantom with power antenna PTE of 1.04%. Data downlink of all 16 valid ASK words has been verified in both unthinned and post-processed implants. LSK uplink at 27Mbps has been verified at a BER of $<1x10^{-4}$, giving energy efficiency of 103pJ/bit for 2.7mW of transceiver power.

Compared with other wireless IMDs that use near-field inductive links, this wireless shank system achieves significantly higher data rates using LSK backscattering. Our data rate is within an order of magnitude of systems utilizing UWB without the power cost of an on-chip power amplifier system or the size of large antenna. While the use of an on-chip inductor does decrease transmission radius, it reduces the volumetric form factor by several orders of magnitude (Table II) [1,2,3,4,5]. This large volume decrease makes integrated Rx coils an attractive option for implantation applications where the available volume is extremely limited but high data rates are still required such as neural recording in small rodents.

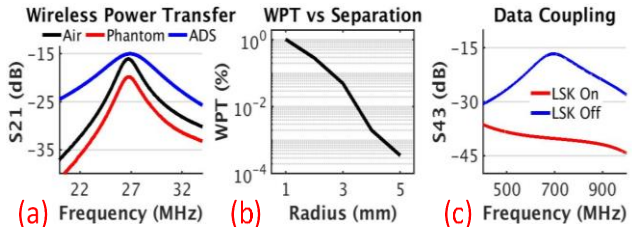

Figure 6. (a) S21 (Tx power to Rx power) measurement data with 1mm air separation (black), with 1mm of gelatin phantom (red), and 1mm air separation simulation for a thinned implant (blue). (b) Peak S21 for coil separation from 1-5mm including a 1mm phantom. (c) S43 (Tx data to Rx data) data with LSK on (red) and LSK off (blue).

Acknowledgment

This work was sponsored in part by the NIH under Grant U01NS099697.

TABLE I. 4-Coil Inductor Parameters

	Power TX	***Power RX***	***Data TX***	***Data RX***
Q_{peak}	58.9	6.1	82.0	5.8
No. Turns	3	5	3	7
D_{out}	4 mm	2 mm	1.6 mm	1.2 mm
F_{sr}	1.75 GHz	1.59 GHz	1.88 GHz	1.48 GHz
L	35 nH	55 nH	15.4 nH	95 nH
R_{Loss}	0.33 Ω	9 Ω	0.91 Ω	82 Ω
K	0.1 (27 MHz)		0.047 (700 MHz)	

TABLE II. Comparison of IMD Transceivers

	[1]	***[2]***	***[3]***	***[4]***	***[5]***	***This Work***
Power Carrier (MHz)	13.56	13.56	13.56	309	-	27
Data Carrier (MHz)	13.56	13.56	50	309	3k-5k	700
Modulation	COOK	PPSK	PDM	LSK	UWB-OOK	LSK
Data Rate (Mbps)	6.78	1.35	13.56	2	67	27
Pow Delivered (mW)	6.3	100	42	0.790	-	4.2
Implant Volume (mm^3)	380[a]	5[a]	45[a]	9.3[a]	-	0.08
Tx/Rx power (pJ/bit)	9.5/-	-	960/162	-/395	30/-	-/103
Techology (nm)	65	600	350	65	90	180
Separation (mm)	35	5-15	10	10	0.5k-4k	1-2.5
BER	9.9e-8	6e-8	4.3e-7	1e-6	1e-8	1e-4

[a.] Assumes implant coils constitute majority of volume and are attached to 220um ultra-thin flex-PCB

References

[1] S. Ha, C. Kim, J. Park, S. Joshi, and G. Cauwenberghs. "Energy recycling telemetry IC with simultaneous 11.5 mW power and 6.78 Mb/s backward data delivery over a single 13.56 MHz inductive link." IEEE JSSC, vol 51, no.11, pp. 2664-2678. Nov 2016.

[2] M. Kiani, and M. Ghovanloo. "A 13.56-Mbps pulse delay modulation based transceiver for simultaneous near-field data and power transmission." IEEE transactions on biomedical circuits and systems, vol. 9, no. 1, pp. 1-11. Feb 2015.

[3] Jiang, Dai, et al. "An integrated passive phase-shift keying modulator for biomedical implants with power telemetry over a single inductive link." IEEE transactions on biomedical circuits and systems, vol. 11, no. 1, pp. 64-77. Feb 2017.

[4] C. Sutardja, and J. Rabaey. "Isolator-less near-field RFID reader for sub-cranial powering/data link of mm-sized implants." IEEE JSSC. Vol 53, no 7, pp. 2032-2042, Jul 2018.

[5] A. Ebrazeh, and P. Mohseni. "30 pJ/b, 67 Mbps, centimeter-to-meter range data telemetry with an IR-UWB wireless link." IEEE Transactions on Biomedical Circuits and Systems vol 9, no. 3 pp 362-369. June 2016.

[6] M. Ghanbari, et al. "A 0.8 mm 3 Ultrasonic Implantable Wireless Neural Recording System With Linear AM Backscattering." IEEE ISSCC. pp 284-286. Feb 2019.